Multipartite entanglement in the Fenna-Matthews-Olson (FMO) pigment-protein complex

A. Thilagam*
Information Technology, Engineering and Environment,
Mawson Institute, University of South Australia, Australia 5095

We investigate multipartite states in the Fenna-Matthews-Olson (FMO) pigment-protein complex of the green sulfur bacteria using a Lorentzian spectral density of the phonon reservoir fitted with typical parameter estimates of the species, P. aestuarii. The evolution of the entanglement measure of the excitonic W qubit states is evaluated in the picosecond time range, showing increased revivals in the non-Markovian regime. Similar trends are observed in the evolution dynamics of the Meyer-Wallach measure of the N-exciton multipartite state, with results showing that multipartite entanglement can last from 0.5 to 1 ps, between the Bchls of the FMO complex. The teleportation and quantum information splitting fidelities associated with the GHZ and W_A resource states of the excitonic qubit channels of the FMO complex show that revivals in fidelities increase with the degree of non-Markovian strength of the decoherent environment. Results indicate that quantum information processing tasks involving teleportation followed by the decodification process involving W_A states of the FMO complex, may play a critical role during coherent oscillations at physiological temperatures.

I. INTRODUCTION

During photosynthesis, the vital processes of light absorption, charge separation and efficient energy transfer to a reaction center (RC) occurs and culminates in the conversion of electronic energy to useful chemical energy [1–6]. These processes are performed by light harvesting (LH) complexes in photosynthetic systems. The well known purple photosynthetic bacteria constitutes two different types of LH system units with ring-like structures, the core LH1 complex which surrounds each RC, and the peripheral LH2 complexes that transfer energy to the LH1 complex [7–9]. While the LH1 complex has only one absorption band at around 875 nm, the LH2 complex may have two absorption bands (800 and 850 nm) in the case of Rhodobacter (Rb.) sphaeroides. In the Fenna-Matthews-Olson (FMO) pigment-protein complex of the green sulfur bacteria, sunlight is transported in the form of electronic energy by bacteriochlorophyll (BChl) molecules to the RC complex [10–15]. Light energy is harnessed with a near efficiencies of 95% [16] or more in natural photosynthetic systems, such efficiencies have yet to be realized in artificial light harvesting complexes. The observation of long lived coherences, lasting several picoseconds, in photosynthetic antenna complexes [13, 17–25] has been linked to quantum entanglement and elements of quantum communication protocols during exciton (correlated electron-hole pair) propagation.

In general, the exciton propagation times between the photosynthetic pigment molecules are about 100 fs. At room temperatures, biological systems undergo large decoherences due to interactions with the surrounding environment, and excitonic coherences are not expected to persist at the comparatively longer times noted in the experimental results. Partly for this reason, there is theoretical interest in the accurate modeling of the dynamics of the exciton to examine the underlying basis for efficient energy transfer in photosynthetic structures. However, the energy scales involved during the energy delocalization and decoherence due to lattice vibrations are almost equivalent $(10-100~{\rm cm}^{-1})$, which makes it a challenging task to model photosynthetic systems. The Markovian approximation in which an infinitely short correlation reservoir time is assumed, provides convenience in computational analysis, but yields reliable results only under certain limiting conditions. Consequently, the exciton hopping model [1, 26, 27] has been replaced by sophisticated quantum mechanical models of exciton propagation incorporating quantum coherence features in recent works [28–34].

While the coupling of the excitonic states to a dissipative environment is expected to lead to fast decoherence, several works have shown that the environment noise can enhance the propagation of energy in light harvesting systems [28, 35–40]. Studies [39–42] have shown that attributes such as the non-Markovian interactions and quantum correlations present in the phonon reservoir help improve the performance of the light harvesting complex. In Ref.[39], Caruso et. al. showed using analysis of the entanglement properties in the Fenna-Matthew-Olson complex, that the delicate interplay of quantum mechanical features and the environmental noise plays a critical role in bringing about

 $^{{\}rm *Electronic~address:~thilaphys@gmail.com}$

an optimal system performance. The authors examined entanglement in further detail in the FMO complex, under different natural and artificial conditions and Markovian and non-Markovian dynamics [40], and showed that near unit energy transfer occurs at the optimal system operating point at which the entanglement measure reaches only intermediate values. In this regard, a thorough examination of the structure and interactions of quantum states in the abstract vector space known as the Hilbert space will contribute to greater insight of optimal processes in photosynthetic systems.

A significant feature of quantum states is their linear structure in Hilbert space. Unusual consequences arise when each quantum state can exist as a sum of two distinctly different states in the tensor product space of the two separate Hilbert subspaces. This unique property underpins many puzzling properties of quantum states, including quantum entanglement which is a valuable resource for the implementation of quantum computation and quantum communication protocols [43–45], which include quantum teleportation [46–48], dense coding [49], quantum cryptography [50, 51] and remote state preparation [52]. Moreover, entanglement effects underpins the emergence of classical macroscopic features in a system undergoing quantum mechanical interactions within itself and with its surrounding environment. The degree of bipartite entanglement of a quantum system which is composed of two subsystems is maximum (minimum) when the constituent subsystems are in completely mixed states (pure states). The well known concurrence measure [53] is zero for separable states, and becomes one when maximal ignorance of each qubit state is achieved in the case of maximally entangled states. A non classical correlation measure known as the quantum discord [54–56] was shown to be non-zero even in non entangled states, and more recently, its q-entropies [57] was shown to incorporate aspects of non-classicality not visible within the conventional definition of the quantum discord.

The exciton manifest as delocalized excitations over the real crystal space [14, 58–62] and thus provides the ideal example of an extended entangled system in molecular systems [63]. To this end, the exciton can be considered to play a central role in the entanglement properties of photosynthetic systems by being in a state of existence at several lattice sites and traversing multiple paths simultaneously. The degree of exciton delocalization is however limited by the fragility of the coupled molecular chromophores interacting with a bath of environmental phonons and static disorder. While the underlying feature that an exciton with a wavevector K is delocalized in real space. is linked with the robustness in quantum coherence during solar energy related biochemical reactions, the exact details of such investigations has yet to be firmly established in current research on exciton propagation in photosynthetic systems . The biggest obstacle to understanding these quantum features is that till now, it is not immediately clear as to how entangled excitonic states act to maintain quantum coherence in photosynthetic processes.

It is important to note the distinction between entanglement measures and those associated with coherences in entangled states which evolve under the influence of environmental variables [64–68]. A global system constituting several subsystem possess entanglement which decays in ways which are vastly different from the coherence of each subsystem, when immersed in a decoherent environment. This stems from the fact that the global characteristics of entangled systems and their evolution under local decoherence differ from those of its constituent subsystems. Entanglement may vanish at a certain finite time prior to the decay of the coherences [64–67, 69], and is a topic of interest as the use of entanglement as a resource is meaningless if it vanishes rapidly. The abrupt disappearance of entanglement at a finite time has been termed entanglement sudden death by Yu et. al. [64]. In general, this finite time is expected to decrease for multipartite states or N-qubit states (N > 2) where several particles are entangled. The relationship between coherence and entanglement remains subtle as decoherence in open quantum systems takes an infinite amount of time to vanish unlike entanglement, however the degree of robustness of the initial state of the quantum system under study is a critical factor that could link entanglement and coherence properties. For instance, it is highly likely that robustly entangled states as initial states are more resistent to decoherence processes.

Unlike bipartite states, investigations related to the robustness of quantum states are challenging for multipartite states, where there is still lack of consensus on the categorization and specification of entanglement itself. Recent works [70, 71] have shown variations in the robustness of different types of multipartite states (Dicke, GHZ, W and cluster states) under decoherence processes. To this end, there has been scant investigations of the characteristics of multipartite states in photosynthetic systems, specifically with respect to the influence of the environmental bath on multipartite excitonic states. The study of multipartite states is particularly relevant for light harvesting systems, as these states possess a richer source of local and nonlocal correlations due to the multitude of partitions available within a group of entangled qubits. Moreover there is relevance in the realistic situation of an entire photosynthetic membrane constituting many FMO complexes and thousands of bacteriochorophylls, possibly giving rise to large cluster of massively entangled excitonic qubits. In this regard, tt would be worthwhile to seek a detailed understanding of how quantum communication protocols [43, 44] such as quantum teleportation [46, 47], are utilized by multipartite states to assist energy transfer in photosynthetic processes. The current work is aimed at addressing some of these issues.

In this work, we consider multipartite entanglement in photosynthetic systems and the decay of these states under decoherence associated with a phonon bath. A characterization of the different types of multipartite entanglement will be examined, including a brief discussion of the robustness of the different types of entanglement against external noise in open quantum system. The influence of specific tasks such as teleportation [46, 47, 72] and quantum state splitting [73, 74] in a noisy photosynthetic system will be examined as well. This work is organized as follows. In Sec. II, we discuss various types of multipartite states and the entanglement quantifiers that are used to characterize some well known multipartite states. In particular, we discuss in detail the global multipartite state entanglement measure, which will be subsequently used to evaluate entanglement quantifiers specific to the FMO complex of P. aestuarii in Sec. III. A description of the photophysics and reaction mechanisms in the Fenna-Matthews-Olson (FMO) complex from the green sulfur bacteria of the two species, Prosthecochloris (P.) aestuarii and Chlorobium (C.) tepidum is provided in Sec. III. In this Section, we also include a detailed evaluation of the exciton-phonon dynamics based on the time-convolutionless (TCL) projection operator technique and a Lorentzian spectral density of the phonon reservoir associated with P. aestuarii. Numerical results of the entanglement measure of the excitonic W states of the FMO complex species P. aestuarii are presented in Sec. III A for both the Markovian and non-Markovian regimes. A similar analysis is performed with respect to the Meyer-Wallach measure of excitonic qubits in the FMO complex in Sec. IV. In Sec. (V), the teleportation and quantum information splitting fidelities of excitonic qubits associated with GHZ and WA resource states, are calculated for the FMO complex species P. aestuarii and the conclusion is provided in Sec. (VI).

II. MULTIPARTITE STATES AND ENTANGLEMENT MEASURES

A qubit state Ψ associated with N>2 subsystems can be written in the multi-qubit state or multipartite state as

$$|\Psi\rangle = \sum_{n=1}^{N} c_n \left(|0\rangle^{\otimes (n-1)} \otimes |1\rangle \otimes |0\rangle^{\otimes (N-n)} \right)$$
 (1)

with coefficients c_n . Multipartite systems generally involve the class of permutation-symmetric states which are invariant when any pair of particles are swapped, and include the Greenberger-Horne-Zeilinger (GHZ) states [75–77] and Dicke states [78]. For a system of N qubits, the Dicke states are obtained using the permutations of basis states with N-K qubits being in the $|0\rangle$ state and K in the $|1\rangle$ state using the notation $|S_{N,K}\rangle$

$$|S_{N,K}\rangle = \binom{N}{K}^{-1/2} \sum_{\text{perm}} \underbrace{|0\rangle \otimes |0\rangle \otimes \cdots |0\rangle}_{N-K} \underbrace{|1\rangle \otimes |1\rangle \cdots |1\rangle}_{K} ,$$
 (2)

where $0 \le K \le N$. A well known example of a symmetric Dicke state with just one excitation is the N-qubit W state [79]

$$|W_N\rangle = \frac{1}{\sqrt{N}} (|100...0\rangle + |01...0\rangle + ... + |0...01\rangle),$$
 (3)

The W states are inequivalent to the GHZ states [67, 76, 77] which are obtained as

$$|GHZ_N\rangle = \alpha \underbrace{|0\rangle \otimes |0\rangle \otimes \cdots |0\rangle}_{N} + \beta \underbrace{|1\rangle \otimes |1\rangle \otimes \cdots |1\rangle}_{N}$$

$$= \alpha |0\rangle^{\otimes N} + \beta |1\rangle^{\otimes N}$$
(4)

where $|\alpha|^2 + |\beta|^2 = 1$. States derived from each other via local operations and classical communication (LOCC) belong to the same group of equivalent resources for quantum information tasks such as quantum teleportation [43]. Consequently, there are differences in robustness against decoherence between entangled W and GHZ states. The W state is known to be highly robust in its genuine multipartite entanglement with respect to loss of a single excitation [79]. However it is still not conclusive whether the W state is more robust against decoherence than the GHZ states, mainly due to the incompatibility in comparison of the dynamics of the two types of states during decoherence. It has been shown that in the case of GHZ states undergoing decoherence [68], the entanglement decay occurs faster when the number of initially entangled particles increases.

Bipartite entanglement are generally quantified by measures such as the von Neumann entropy [80, 81], negativity [45, 82], concurrence [53] and quantum discord [54–56]. These measures cannot be extended to the case of multipartite system without introducing an element of subjectivity associated with the partitioning of the global system into smaller systems. As a consequence different entanglement measures are expected to display variations in their decay under decoherence. Currently, there exists several entanglement measures, such as the the Meyer and Wallach measure [83]

and its extension based on the normalized negativity which are used to quantify multipartite entanglement. In a recent work, Chaves et. al. [84] identified entanglement measures of states undergoing decoherence with tasks such as teleportation [46, 47] and the splitting [73, 74] of quantum information. Thus in this elegant approach, a task associated with quantum information processing was associated with the entanglement quantifiers.

A commonly adopted approach that is used to determine the multipartite entanglement measure of a N-qubit state first involves partitioning it $2^{N-1}-1$ times. Subsequently, a bipartite entanglement measure such as the von Neumann entropy [80, 81] or negativity [45] can be evaluated for each bi-partitioned density matrix. The average of the sum of the entropies or negativities over all possible partitions may be used to characterize the global entanglement. In connection with this, we adopt the global multipartite state entanglement measure used in Ref.[71]

$$E = \frac{1}{[N/2]} \sum_{m=1}^{[N/2]} E^{(m)}, \tag{5}$$

$$E^{(m)} = \frac{1}{N_{bi}^m} \sum_{i=1}^{N_{bi}^m} E(i). \tag{6}$$

where E(i) denotes the entanglement associated with a single bipartition of the N-qubit system and $E^{(m)}$ denotes the average entanglement between subsets of m qubits and the remaining N-m qubits. The average is performed over the $N_{bi}^{(m)}$ nonequivalent bipartitions, $N_{bi}^{m} = \binom{N}{n}$ if $n \neq N/2$ and $N_{bi}^{N/2} = \frac{1}{2} \binom{N}{N/2}$ if n = N/2. The total number of bipartitions is equal to $N_{cuts} = \sum_{i=1}^{[N/2]} N_{bi}^{i} = 2^{N-1} - 1$. Due to the occurrence of mixed states, the negativity is employed as a suitable measure of bipartite entanglement. The normalized negativity is defined as [85]

$$E(i) = \frac{2}{2^m - 1} \sum_{i} |\alpha_i|,\tag{7}$$

where α_i is the negative eigenvalue of the partial transpose matrix for m and the remaining N-m bipartition. The measures in Eqs. (6) and (7) will be employed in the next section to evaluate the entanglement dynamics of the excitonic qubits in the FMO complex.

III. EXCITONIC QUBITS IN THE FMO COMPLEX

In this Section, we examine the exciton entanglement dynamics of the Fenna-Matthews-Olson (FMO) complex from the green sulfur bacteria of the two species, *Prosthecochloris (P.) aestuarii* and *Chlorobium (C.) tepidum* based on semiempirical values of the reservoir characteristics at cryogenic temperatures [86]. Fig. 1 shows a simplified light reaction scheme in which photons are absorbed by a network of antenna pigments linked to the FMO complex, and from which the excitation energy is transported to the reaction center (RC) where photochemical reactions convert the excitation energy into chemical energy. The FMO complex trimer, which constitutes three identical monomer subunits with each unit constituting seven bacteriochlorophyll (BChl)a molecules, acts as an efficient channel of energy propagation from the light harvesting molecular complex to the reaction center.

In the experimental work [86], FMO complexes from Prosthecochloris (P.) aestuarii and Chlorobium (C.) tepidum were isolated and dissolved in suitable solvents before time-resolved transient absorption measurements were performed. The site energies and coupling between each BChla molecules of Prosthecochloris (P.) aestuarii and Chlorobium (C.) tepidum were characterized Ref. [86–88] using an effective exciton model [87], which accounts well for the optical steady state spectra and the dynamics of the FMO complexes. For both species of FMO complexes, the third BChl (numbered 3 in Fig. 1) was found to have the lowest site energy [86]. However there are subtle differences between the two species as the absorption spectrum of P. aestuarii has an absorption spectrum maximum height at 815 nm, while that of the C. tepidum has its maximum at 806 nm. In P. aestuarii, BChls 1 and 4 contribute to the 815 nm absorption spectrum band whereas the contribution to the same band arises mainly from BChl 4 in C. tepidum. Consequently, we expect differences in the coherence features that can arise when these two species are coupled to a phonon bath with similar environmental parameters.

In Table I, the Bchl site energies for the FMO complex of P. aestuarii (cm⁻¹) given in Refs. [14], [86] and [15] are provided. The difference in site energies (provided within $\{\ \}$) is calculated via subtraction from the site energy of the third BChl. It is important to distinguish the propagating exciton from the presence of excitation at a specific Bchl site, as it is well known that an exciton with a wavevector \mathbf{K} is delocalized in real space. The qubit state has a probabilistic occupation at all the BChl sites, with one or two BChl sites contributing predominantly to the qubit state. We use an effective exciton Hamiltonian defined in the basis of the \mathbf{Q}_y one-exciton states in which the

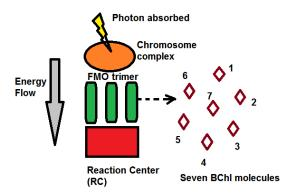


FIG. 1: Simplified scheme of the light reaction in which photons are absorbed by a network of antenna pigments linked to the FMO complex, and from which the excitation energy is transported to the reaction center (RC). Photochemical reactions take place at the RC to convert the excitation energy into chemical energy.

TABLE I: The Bchl site energies (cm⁻¹) used in Refs. [14] (provided as true values of the site energies in last column of Table 3), [15] and [86] for the FMO complex of *P. aestuarii*. The difference in site energies (provided within { }) is calculated by considering the site energy of the third BChl as a reference point.

BChl	Exciton energy (cm^{-1}) [86]	Exciton energy (cm^{-1}) [14]	Exciton energy (cm^{-1}) [15]
3	12,112 {0 }	12,210 {0}	12,175 {0}
1	$12,266 \{154\}$	12,450 {240}	12,315 {140}
4	12,293 {181}	12,320 {110}	12,405 {230}
6	12,396 {284}	12,540 {330}	12,430 {255}
7	12,457 {345}	12,470 {260}	12,450 {275}
2	12,496 {384}	12,520 {310}	12,500 {325}
5	$12,634 \{522\}$	12,550 {340}	12,625 {450}

 Q_y bandwidth is associated with the lowest excited state of the BChl molecule. When a photon is absorbed by the BChl molecule, the newly created exciton propagates rapidly to the adjacent units while interacting with a bath of phonons. The exciton can be considered as delocalized over all the seven BChls so that the excitonic states are obtained as linear combinations of the excited state wave functions of the individual BChl. In this regard, a simple way to represent excitonic states as qubit states is by associating a qubit with the presence (or absence) of an exciton at a specific energy level. Each energy level can be modeled as a two-level system, with $|0\rangle_{e_1}$ ($|1\rangle_{e_1}$) denoting the absence (presence) of an excitation at the specified energy level.

In order to compute the contributions from different pigments to the seven exciton states, we model the subunit of the FMO complex via the Hamiltonian, \hat{H}_{ex} in the site basis, with the coupling energy terms given in units of cm⁻¹

$$\hat{H}_{ex} = \begin{pmatrix} 240.0 & -104.1 & 5.1 & -4.3 & 4.7 & -15.1 & -7.8 \\ -104.1 & 310.0 & 32.6 & 7.1 & 5.4 & 8.3 & 0.8 \\ 5.1 & 32.6 & 0 & -46.8 & 1.0 & -8.1 & 5.1 \\ -4.3 & 7.1 & -46.8 & 110.0 & -70.7 & -14.7 & -61.5 \\ 4.7 & 5.4 & 1.0 & -70.7 & 340.0 & 89.7 & -2.5 \\ -15.1 & 8.3 & -8.1 & -14.7 & 89.7 & 330.0 & 32.7 \\ -7.8 & 0.8 & 5.1 & -61.5 & -2.5 & 32.7 & 260.0 \end{pmatrix}.$$

$$(8)$$

The off-diagonal terms in \hat{H}_{ex} are obtained using the intersite excitonic couplings between various BChls as given in Ref.[14] for the FMO complex of P. aestuarii. The various coupling energies were evaluated [14] in a dielectric

TABLE II: Delocalized exciton qubit states provided as linear combinations of probability occupation amplitudes associated with the seven BChl sites. The excitonic qubit states are labeled according to increasing exciton energies for the FMO complex of *P. aestuarii*.

	$ 1\rangle_{e_1}$	$ 1\rangle_{e_2}$	$ 1\rangle_{e_3}$	$ 1\rangle_{e_4}$	$ 1\rangle_{e_5}$	$ 1\rangle_{e_6}$	$ 1\rangle_{e_7}$
$E_x (\mathrm{cm}^{-1})$	-24	86	167	251	280	385	444
BChl 1	0.0553	0.0750	0.8081	-0.0444	-0.0305	0.5688	0.1087
BChl 2	0.1155	0.0609	0.5555	-0.1127	-0.0950	-0.7943	-0.1475
BChl 3	-0.9062	-0.3811	0.1314	-0.1119	0.0214	-0.0515	-0.0232
BChl 4	-0.3903	0.8121	-0.0124	0.3431	-0.1501	-0.0722	0.2061
BChl 5	-0.0730	0.2644	-0.0992	-0.4529	-0.4445	0.1860	-0.6911
BChl 6	-0.01267	-0.1020	0.1048	0.7200	0.2077	0.0561	-0.6432
BChl 7	-0.0662	0.3249	0.0081	-0.3627	0.8522	0.0038	-0.1793

environment by solving a Poisson equation for each BChl by a finite difference method. The diagonal terms of \hat{H}_{ex} in Eq. (8) were obtained using the energy differences for the respective BChl site using the site energies, provided within $\{\ \}$, in Table I. The exciton energies and eigenstates of \hat{H}_{ex} in Eq. (8) can be evaluated using standard diagonalization techniques. The seven excitonic qubits (labelled in order of increasing energy) are given in Table II. It can be seen that each exciton state is generally associated with 1-3 Bchl sites, and the lowest energy exciton qubit state $|1\rangle_{e_1}$ with energy $-24~{\rm cm}^{-1}$ is localized mostly on BChls 3 and 4. Most importantly, Table II shows that each exciton qubit state may have simultaneous occupation of two or more BChl sites, a feature that is only feasible in quantum systems.

In general, the dimer model consisting of pair of spin-boson [89] can be used to simplify analysis of the entanglement dynamics of the excitonic qubits. The spin-boson system is a well known quantum dissipative system which constitutes two energy levels that couple to an infinite system of harmonic oscillators. The case of the multipartite entanglement can be examined by extending the global system to several spin chains. We model each two-level excitonic qubit interacting with phonons via the Hamiltonian,

$$H = \omega_0 \sigma_+ \sigma_- \sum_{\mathbf{q}} \hbar \omega_{\mathbf{q}} b_{\mathbf{q}}^{\dagger} b_{\mathbf{q}} + \sum_{\mathbf{q}} \lambda_{\mathbf{q}} \left(\sigma_- b_{\mathbf{q}}^{\dagger} + \sigma_+ b_{\mathbf{q}} \right), \tag{9}$$

where $\sigma_{+} = |1\rangle\langle 0|$ and $\sigma_{-} = |0\rangle\langle 1|$, are the respective Pauli raising and lowering operators of the exciton with transition frequency, ω_{0} .

In order to utilize Eqs. (6) and (7) for further analysis of the excitonic qubits, and to keep the problem tractable, we assume that each qubit is coupled to its own reservoir of phonons. The phonon reservoir is given by the second term on the right hand side of Eq. (9) where $b_{\bf q}^{\dagger}$ and $b_{\bf q}$ are the respective phonon creation and annihilation operators with wave vector ${\bf q}$. The last term of Eq. (9) denotes the qubit-oscillator interaction Hamiltonian which we assume to be linear in terms of the phonon operators. $\lambda_{\bf q}$ is the coupling between the qubit and the environment and is characterized by the spectral density function, $J(\omega) = \sum_{\bf q} \lambda_{\bf q}^2 \delta(\omega - \omega_{\bf q})$.

For the spectral density associated with the coupling of the BChl exciton to the phonon bath environment, we

For the spectral density associated with the coupling of the BChl exciton to the phonon bath environment, we consider a Lorentzian spectral density of the reservoir fitted with estimates derived from site-selective fluorescence measurements on the 825 nm band of the FMO complex of *P. aestuarii* [86]

$$J(\omega) = \frac{1}{2\pi} \gamma_0 \left(\frac{\Delta\omega}{2}\right)^2 \frac{1}{(\omega_0 - \delta - \omega)^2 + \left(\frac{\Delta\omega}{2}\right)^2}$$
(10)

whose central peak is detuned from the exciton transition frequency ω_0 by an amount δ which is treated as a parameter for subsequent analysis. It important to distinguish between the molecular transition frequency associated with the Q_y band of the Bchl-a molecular system (about 12100cm^{-1} , see Table I) and the actual excitonic energies which are of the order of the typical binding energies of 0.1-0.2 eV in organic molecules [59]. We consider that the phonon modes have maximum energies just enough to convert the exciton into free electron-hole pairs, however in general the greater involvement of a lower range of phonon energies of the order 0.01 eV (or 80 cm^{-1}) is assumed. As a standard, we use the full width at half-maximum $\Delta \omega = 80 \text{ cm}^{-1}$ as used in Ref.[86], noting that the width is related to the reservoir correlation time τ_B via $\Delta \omega = \frac{2}{\tau_B}$. However in order to examine the influence of the reservoir correlation time τ_B on population differences, we parameterize $\Delta \omega$ around the region where phonon energies lie close to 80 cm^{-1} .

The parameter γ_0 is associated with the relaxation time scale τ_R of the exciton via the relation $\tau_R = \gamma_0^{-1}$, and $\gamma_0 = 111 \mathrm{ps}^{-1}$ was used in Ref. [86]. γ_0 , is expected to increase with temperature, hence for subsequent calculations, this term will be treated as a parameter. While the conditions under which the experimental work in Ref. [86] was carried out precludes significant temperature-dependent dephasing processes, we consider higher values of γ_0 (1000 to 2000 cm⁻¹) to incorporate non-Markovian effects. Hence we assume that the spectral density profile in Eq. (9) holds valid at higher temperatures (> 50 K).

Due to the exciton-phonon interactions, the excitonic qubit decays to oscillator states in the reservoir, making a transition from its excited state $|1\rangle_e$ to ground state $|0\rangle_e$. We assume an initial state of the qubit with its corresponding reservoir in the vacuum state of the form [90]

$$|\phi_i\rangle = |1\rangle_e \otimes \prod_{k=1}^{N'} |0_k\rangle_{\rm r} = |1\rangle_e \otimes |0\rangle_{\rm r},$$
 (11)

where $|0\rangle_{\rm r}$ implies that all N' wavevector modes of the reservoir are unoccupied in the initial state. The subscripts e and r refer to the excitonic qubit and the corresponding reservoir respectively. $|\phi_i\rangle$ undergoes subsequent decay of the following form

$$|\phi_i\rangle \longrightarrow u(t) |1\rangle_e |0\rangle_r + v(t) |0\rangle_e |1\rangle_r,$$
 (12)

In order to keep the problem tractable we consider that $|1\rangle_r$ denotes a collective state of the reservoir as follows

$$|1\rangle_{\mathbf{r}} = \frac{1}{v(t)} \sum_{n} \lambda_{\{n\}}(t) |\{n\}\rangle, \tag{13}$$

where $\{n\}$ denotes an occupation scheme in which there are n_i oscillators with wavevector k=i in the reservoir and we define the state $|\{n\}\rangle$ as [90]

$$|\{n\}\rangle = |n_0, n_1, n_2...n_i..n_{N'}\rangle,$$
 (14)

In the collective reservoir state, the phonon oscillators can be present at all allowed modes, including simultaneous excitation of several phonon states. At non-zero temperatures, the reservoir state is a Boltzmann weighted average over all possible permutations of the occupation scheme $\{n\}$.

Following the time-convolutionless (TCL) projection operator technique described in Chapter 10 of Ref.[91], we obtain an expression for the coefficient u(t) (see Eq. (11)),

$$\dot{u}(t) = -\int_{0}^{t} \int d\omega J(\omega) \exp[i(\omega_0 - \omega)(t - t_1)] u(t_1) dt_1, \tag{15}$$

which can be solved by means of a Laplace transformation. The time-convolutionless projection operator technique is independent of the choice of the spectral density of the environment and accounts for strong non-Markovian dynamics [91], that may arise in the photosynthetic molecular environment.

Eq. (15) is further simplified using the form of spectral density in Eq. (10)

$$\dot{u}(t) = -\int_{0}^{t} \frac{1}{2} \gamma_0(\Delta \omega / 2 - i\delta) e^{-(\Delta \omega / 2 - i\delta)|t - t_1|} u(t_1) dt_1, \tag{16}$$

The Laplace transformation of Eq. (15) with initial condition u(0) = 1, yields the solution [91]

$$u(t) = e^{-(\Delta\omega/2 - i\delta)t/2} \left[\cosh\left(\frac{\xi t}{2}\right) + \frac{\Delta\omega/2 - i\delta}{\xi} \sinh\left(\frac{\xi t}{2}\right) \right],\tag{17}$$

where $\xi = \sqrt{(\Delta\omega/2 - i\delta)^2 - \gamma_0 \Delta\omega}$. Fig. 2a,b,c illustrates the evolution of the coherence properties as reflected in the exciton population difference, ΔP between the excited state $|1\rangle_e$ and ground state $|0\rangle_e$, evaluated using $|u(t)|^2$ (Eq. (17). The change of ΔP with time t (ps), $\Delta\omega/2$ and γ_0 shows that for smaller $\Delta\omega/2 \sim 20$ cm⁻¹ (or larger reservoir correlation time) and large γ_0 (or small exciton relaxation times), there is increased time period (up to 1 ps) over which the population difference, ΔP which is a signature of coherence, is maintained for a select range of parameters. The time duration of effective coherence (about 1 ps) obtained here appear to compare well with times of population transfer between various exciton levels (about 1 ps for levels 1 and 2) noted for the FMO complex of P. aestuarii [86]. These results suggest that the non-Markovian regime is best suited for occurrence of large coherence times. The analytical form for u(t) in Eq. (17) will be useful for further analysis of the entanglement measure for the W states of the FMO complex which we describe next.

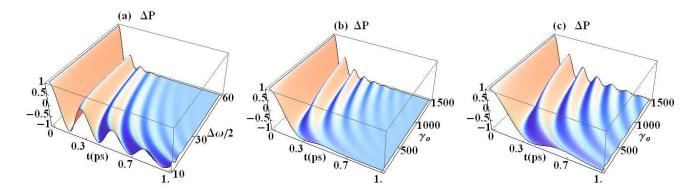


FIG. 2: (a) The population difference, ΔP between the excited state $|1\rangle_e$ and ground state $|0\rangle_e$, evaluated using $u(t)^2$ (Eq. (17), as a function of time t (ps) and $\Delta \omega/2$ (cm⁻¹) at $\gamma_0=1000$ cm⁻¹ and detuning parameter, $\delta=0$. (b) ΔP as a function of time t (ps) and γ_0 (cm⁻¹) at $\Delta \omega/2=40$ cm⁻¹. (c) ΔP as a function of time t (ps) and γ_0 (cm⁻¹) at $\Delta \omega/2=20$ cm⁻¹.

A. Entanglement dynamics of excitonic W states of the FMO complex

We consider a system of four non-interacting excitonic qubits coupled to uncorrelated reservoirs and which are initially prepared in the W state as follows

$$|\phi_{0}\rangle = (|0001\rangle_{e_{1}e_{2}e_{3}e_{4}} + |0010\rangle_{e_{1}e_{2}e_{3}e_{4}} + |0100\rangle_{e_{1}e_{2}e_{3}e_{4}} + |1000\rangle_{e_{1}e_{2}e_{3}e_{4}} + |1000\rangle_{e_{1}e_{2}e_{3}e_{4}}|0000\rangle_{r_{1}r_{2}r_{3}r_{4}}/2,$$

$$(18)$$

The system of four qubit state is a reasonable compromise between a high number of entangled states and resource available for numerical computations. The evolution of the total system can be obtained using Eq. (12), so that a typical form of the following term evolves as

$$|1\rangle_{e_{1}}|0\rangle_{e_{2}}|0\rangle_{e_{3}}|0\rangle_{e_{4}}|0\rangle_{r_{1}}|0\rangle_{r_{2}}|0\rangle_{r_{3}}|0\rangle_{r_{4}} \longrightarrow \left[u_{1}(t)|1\rangle_{e_{1}}|0\rangle_{r_{1}}+v_{1}(t)|0\rangle_{e_{1}}|1\rangle_{r_{1}}\right]|0\rangle_{e_{2}}|0\rangle_{e_{3}}|0\rangle_{e_{4}}|0\rangle_{r_{2}}|0\rangle_{r_{3}}|0\rangle_{r_{4}},$$

where $u_1(t)$ and $v_1(t)$ (see Eqs.(12), (17)) are interaction parameters associated with the first excitonic qubit which we label via the subscript 1. Continuing with the same manner with the remaining three excitonic qubits, we obtain

$$|\phi_{t}\rangle = [|000\rangle_{e_{1}e_{2}e_{3}}|000\rangle_{r_{1}r_{2}r_{3}}(u_{4}(t)|1\rangle_{e_{4}}|0\rangle_{r_{4}} + v_{4}(t)|0\rangle_{e_{4}}|1\rangle_{r_{4}}) + |000\rangle_{e_{1}e_{2}e_{4}}|000\rangle_{r_{1}r_{2}r_{4}}(u_{3}(t)|1\rangle_{e_{3}}|0\rangle_{r_{3}}) + v_{3}(t)|0\rangle_{e_{3}}|1\rangle_{r_{3}}) + |000\rangle_{e_{1}e_{3}e_{4}}|000\rangle_{r_{1}r_{3}r_{4}}(u_{2}(t)|1\rangle_{e_{2}}|0\rangle_{r_{2}}) + v_{2}|0\rangle_{e_{2}}|1\rangle_{r_{2}}) + |000\rangle_{e_{2}e_{3}e_{4}}|000\rangle_{r_{2}r_{3}r_{4}}(u_{1}(t)|1\rangle_{e_{1}}|0\rangle_{r_{1}} + v_{1}(t)|0\rangle_{e_{1}}|1\rangle_{r_{1}})]/2.$$
(20)

The reduced density operator of the excitonic qubit subsystem $\rho_e(t) = \text{Tr}_r(|\phi_t\rangle \langle \phi_t|)$ and the reduced density operator of reservoir subsystem $\rho_r(t) = \text{Tr}_e(|\phi_t\rangle \langle \phi_t|)$ can be obtained, provided details of each individual system-reservoir parameters, u_i, v_i (i=1-4) are known. The detailed derivation of the density operator matrices for such generalized exciton-phonon reservoir systems is complex and for ease in numerical evaluations, we consider the simple model in which $u_1 = u_2 = u_3 = u_4 = u$. Thus each of the exciton is assumed to be coupled to a independent phonon bath, with same spectral density. This allows convenient evaluation of the entanglement measure of the excitonic qubit (denoted by E_e) and phonon reservoir E_r systems, using Eqs.(5) and (7), and at the same time is not a significant compromise on the accuracy of the evaluated results. Three parameters which appear in the spectral density relation in Eq.(10) are expected to play critical role in the analysis of the entanglement dynamics, (a) time (t), (b) γ_0 which is associated with the exciton relaxation time and (c) δ which is the amount by which the central peak is detuned from the exciton transition frequency.

We consider both the Markovian $(\Delta \omega \gg \gamma_0)$ and non-Markovian regimes $(\Delta \omega \ll \gamma_0)$ as well as the non- resonant case for which $\delta \neq 0$. Fig. 3a,b illustrates the evolution of the entanglement measure of the excitonic qubit subsystem (reservoir subsystem), E_e (E_r) as function of time t (in picoseconds) and γ_0 (in units of cm⁻¹). The entanglement measures are evaluated for the W state (Eq.(18) using Eqs.(5), (7) and (17), and setting the detuning parameter at $\delta = 0$. It can be seen that as γ_0 increases, the sub-systems move into the non-Markovian regimes, and increased oscillations in revivals of entanglement, associated with comparatively long phonon reservoir correlation times, can

be seen in both sub-systems. The non-Markovian features are expected due to inflow of quantum information from the reservoir subsystem back into the excitonic qubit subsystem. Overall there is net flow of entanglement from the excitonic subsystems to the phonon reservoir systems after 0.5 ps. Fig. 3c also illustrates that for smaller $\Delta\omega/2 \sim 20$ cm⁻¹ where there is higher reservoir correlation time, there is a pronounced revival in the entanglement measure E_e .

Figs. 4a,b also show that both the entanglement measures, E_e and E_r decrease when the detuning δ increases, which has been attributed to the effective decrease in coupling between the two interacting subsystems [92]. The time duration for which significant entanglement exists ($\approx 0.1\text{-}0.3$ ps) obtained here is less than the decoherence times noted for the FMO complex of P. aestuarii [86]. The evaluation of the entanglement measures, E_a and E_r based on GHZ states are expected to yield similar qualitative variations with respect to change in time t, γ_0 and δ as obtained for the W states. However some quantitative differences due to the different degree of robustness of the different multipartite states, can be expected in the entanglement measures, E_a and E_r .

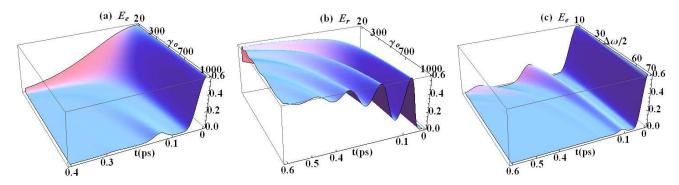


FIG. 3: (a) Entanglement measure of the excitonic qubit subsystem, E_e as function of time t (ps) and γ_0 (cm⁻¹), evaluated for the W state (Eq.(18) using Eqs.(5) and (7). The detuning parameter, $\delta = 0$. $\Delta \omega = 80$ cm⁻¹ [86] in Eq.(10). The parameter estimates are typical of the FMO complex of P. aestuarii [86]—(b) Same as in (a) except that the entanglement measure of the system of the collective reservoir states E_r is obtained as a function of t (ps) and γ_0 (cm⁻¹)—(c) Entanglement measure of the excitonic qubit subsystem, E_e as function of time t (ps) and $\Delta \omega / 2$ (cm⁻¹), with the detuning parameter, $\delta = 0$ and $\gamma_0 = 1000$ cm⁻¹.

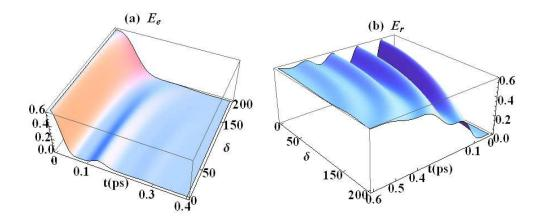


FIG. 4: (a) Entanglement measure of the excitonic qubit subsystem, E_e as function of time t (ps) and δ (cm⁻¹), evaluated for the W state (Eq.(18) using Eqs.(5) and (7). γ_0 is set at 1000 cm⁻¹ and $\Delta\omega/2=40$ cm⁻¹. (b) Same as in (a) except that the entanglement measure of the system of the collective reservoir states E_r is obtained as a function of t (ps) and δ (cm⁻¹)

It is important to note that the results obtained here are based on simplified model systems with underlying assumptions, such as the requirement that all qubits in different Hilbert subspaces experience similar isotropic interactions with the phonon reservoir subsystem. The qubits are assumed to be independent of each other, and coupled to uncorrelated reservoirs. In the realistic situation, each excitonic qubit may share one or more BChl sites as shown in Table II, which means that the reservoir subsystems are correlated as well. Due to the large energy difference between each qubit system (about 100 cm⁻¹, Table II), the energy profile of phonon modes linked to different qubit are expected to be different, which to some extent justifies the assumption that the reservoir system are uncorrelated. The

basic models employed here also circumvent the inclusion of more realistic features such the correlated fluctuations of the exciton transition energies. It has been shown that environmental changes lead to correlated fluctuations of the exciton transition and interaction energies with impact on population transfer rates, decoherence rates and the efficiency of photosynthetic complexes [25]. Even interaction fluctuations of a small magnitude results in an increase in efficiency of the FMO complex [25]. Nevertheless, the use of the assumptions mentioned earlier have enabled the numerical evaluation of some estimates of the timescales involved in the entanglement dynamics of the system under study, and to help understand on a qualitative level some critical parameters responsible for quantum coherence in light-harvesting systems. The incorporation of realistic features will lead to slight changes in the magnitude of the entanglement measures considered here and in the next Section, however the qualitative features are expected to be retained.

IV. MEYER-WALLACH MEASURE OF EXCITONIC QUBITS IN THE FMO COMPLEX

In this section, we evaluate the Meyer-Wallach measure for a system of photosynthetic qubits, with each qubit interacting with its own reservoir of phonons. This monotone measure was defined by Meyer and Wallach [83] as a single scalar measure of pure state entanglement for a system of more several qubits. For the case of N qubits, the Meyer-Wallach measure is based on the entanglement of each qubit with the remaining (N-1)-qubits as follows

$$Q = \frac{1}{N} \sum_{k=1}^{N} 2(1 - \text{Tr}[\rho_k^2]), \tag{21}$$

where ρ_k is the reduced density matrix of the kth qubit obtained after tracing out all the remaining qubits. The Meyer-Wallach measure has inherent deficiencies in that it is unable to distinguish states which are fully inseparable from states which are separable into states of subsystems. Nevertheless, it is a useful qualitative measure in the investigation of subtle features of entangled systems, and which we will utilize to analyze the dynamics of the photosynthetic system under study in this Section.

We first consider the joint evolution of a pair of non-interacting excitonic qubits coupled to uncorrelated phonon reservoirs, and which are initially prepared in the following state

$$|\phi_0\rangle = [a(|00\rangle_{e_1e_2} + b|11\rangle_{e_1e_2}] |00\rangle_{r_1r_2},$$
 (22)

The state above evolves as a four-qubit multipartite state influenced by the real coefficients a, b. There are obvious differences between the entangled states in Eq.(22) and (18). The density matrix of the excitonic subsystem derived from the global state in Eq.(22) and expressed within the basis $(|0 0\rangle, |0 1\rangle |1 0\rangle |1 1\rangle)$ appear as

$$\rho_{e_1,e_2}(t) = \begin{pmatrix} f_1(t) & 0 & 0 & f_5(t) \\ 0 & f_2(t) & 0 & 0 \\ 0 & 0 & f_3(t) & 0 \\ f_5(t) & 0 & 0 & f_4(t) \end{pmatrix}. \tag{23}$$

. For $t \geq 0$, the matrix elements of the matrix appearing in Eq.(23) evolve as

$$f_1(t) = a^2 + b^2 v_1(t)^2 v_2(t)^2,$$

$$f_2(t) = b^2 v_1(t)^2 u_2(t)^2,$$

$$f_3(t) = b^2 u_1(t)^2 v_2(t)^2,$$

$$f_4(t) = b^2 u_1(t)^2 u_2(t)^2,$$

$$f_5(t) = a b u_1(t) u_2(t).$$

where u_i, v_i are conversion functions associated with the *i*th exciton and its phonon reservoir. The problem can be extended to the photosynthetic system examined earlier by substituting u with the form obtained in Eq.(17). It should be noted that the X-state structure in Eq.(23) preserve its X-form during evolution.

For density matrix given in Eq. (23), an explicit expression of the Meyer-Wallach measure for the N-exciton multipartite state is obtained as [90, 93]

$$Q = 2a^2b^2 + 4b^2u^2v^2 (24)$$

where it is assumed that $u_i = u$ for all the N exciton-reservoir interacting system. Due to this assumption, the Meyer-Wallach measure, Q in Eq.(24) is independent of N. For the elaborate and more realistic models, in which some

exciton-reservoir systems evolve differently from adjacent pairs, Q becomes a complicated function of the differences in system-reservoir dynamics in separate Hilbert subspaces. For this reason, we chose a highly simplified scenario of the same mode of exciton-reservoir for all N qubits, as was also the case in Sec. III A.

Substituting the form of u given in Eq.(17) into Eq.(24), the evolution dynamics of the Meyer-Wallach Q measure is plotted in Fig. 5a,b. The figure shows expected differences between the Q measure and the entanglement measures E_e and E_r obtained in the preceding Section. Unlike E_e , the Q measure incorporates the entanglement of the global system which constitutes the reservoir subsystems as well. As a consequence, the magnitude of Q shows slower decay with time t at large $\gamma_0 \approx 800 cm^{-1}$ as seen in Fig. 5a. Q is also sensitive to the correlation parameters a and b (see Eq.(22)) as illustrated in Fig. 5b. As in the case of the entanglement measures E_e and E_r , there is increased revivals in entanglement as the degree of non-Markovian strength increases. These revivals can be seen as a signature of coherence, and hence the correlation parameter b plays a critical role in the length of time over which such revivals can be maintained. In general, the maximum Q = 1 is obtained for a = 0, b = 1 with $u_1 = u_2 = \frac{1}{\sqrt{2}}$.

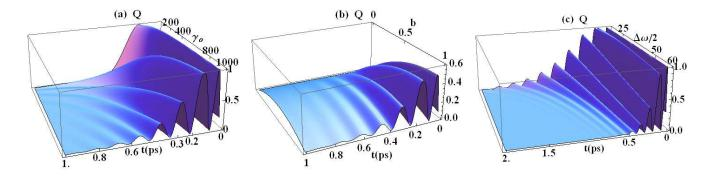


FIG. 5: (a) MeyerWallach measure Q (Eq.(24)) as a function of time t (ps) and γ_0 (cm⁻¹), evaluated for the state in Eq.(22) using Eq. (24). a=0, b=1 and $\Delta\omega/2$ =40 cm⁻¹. (b) MeyerWallach measure Q as a function of time t (ps) and parameter b, γ_0 =800 cm⁻¹ and $\Delta\omega/2$ =40 cm⁻¹. (c) Meyer Wallach measure Q as a function of time t (ps) and $\Delta\omega/2$, γ_0 =1000 cm⁻¹, a=0, b=1.

V. TELEPORTATION AND SPLITTING FIDELITIES OF EXCITONIC QUBITS IN THE FMO COMPLEX

In this section, we apply the results of teleportation fidelities obtained by Chaves et. al. [84] to analyze the entanglement dynamics of the FMO complex detailed in Sec. III. Using the concept that multipartite entanglement is linked to the teleportation and quantum information splitting protocols [84], we examine the effect of the phonon reservoir on the entanglement properties of the excitonic qubits in the FMO complex. This is also linked to the possibility that the entangled qubit states in the photosynthetic complex may act as a resource for the teleportation and quantum information splitting protocols.

In the teleportation process [46–48], two parties conventionally referred to as Alice and Bob share an entangled bipartite state, with the quality of the teleportation measured by the fidelity $f = \langle \psi | \rho | \psi \rangle$, where ρ is the state obtained after teleportation of an unknown quantum state $|\psi\rangle$. For the unknown state of dimension d, the maximum achievable fidelity f_{max} for a given bipartition of the state used as the medium of transmission is [84] $f_{\text{max}} \leq \frac{2+2\mathcal{N}}{d+1}$ where the negativity \mathcal{N} is associated with the given bipartition. The bipartite mixed state leads to imperfect teleportation, and thus reduce the fidelity of teleportation to values below those of the pure states which yield a fidelity of $\frac{2}{3}$ [48].

Chaves et. al. [84] considered a viable connection between global entanglement quantifiers in entangled systems and the robustness of tasks such as teleportation and the splitting of quantum information [73, 74], which is a generalization of the teleportation protocol. During the splitting process, an unknown qubit $|\Psi_0\rangle = \cos{(\theta/2)} |0\rangle + e^{i\phi} \sin{(\theta/2)} |1\rangle$ is sent to N other parties via a shared entangled state. The no-cloning theorem ensures that only a single copy of $|\Psi_0\rangle$ can be retrieved. The association between the degree of cooperation of the N parties during the extraction process and the global entanglement of the shared GHZ or W-like states under decoherence were examined in Ref.[84]. The results that is of particular relevance in the context of photosynthetic systems, are the explicit forms of teleportation and quantum information splitting fidelities obtained in Ref.[84] for protocols associated with GHZ and W_A states, under the amplitude-damping channel. The W_A state is associated with N+1 qubits and of the form

$$\left|W_A^{N+1}\right\rangle = \frac{1}{\sqrt{2}} \left[\left|0\right\rangle \left|W_N\right\rangle + \left|1\right\rangle \left|0\right\rangle^{\otimes N} \right],\tag{25}$$

We note the similarities between the amplitude-damping channel and the action of the phonon reservoir on the photosynthetic qubit as detailed in Sec. III. Within this channel, the population of the excited state is reduced by a factor 1-p, where the p is a parameterization of time. For the excitonic qubit interacting with a phonon bath, one has $p=1-|u(t)|^2$, where u(t) appears in Eq. (17). At initial time t=0, u(t)=1 and p=0, and at $t\to\infty$, u(t)=0 and p=1.

The teleportation fidelity, averaged over all the possible input states $|\Psi_0\rangle$, was obtained as [84]

$$F_{GHZ} = \frac{1}{6} \left[2 + (1-p)^{N-1} (2-p) + 2 (1-p)^{N/2} + p^{N-1} (1+p) \right]$$
 (26)

for GHZ resource states. In the case of the W_A state associated with N+1 qubits, $|W_A^{N+1}\rangle = \frac{1}{\sqrt{2}} \left[|0\rangle |W_N\rangle + |1\rangle |0\rangle^{\otimes N} \right]$, the teleportation fidelity was obtained as [84]

$$F_W = \frac{1}{3} \left(3 - 2p + p^2 \right) \tag{27}$$

Chaves. et. al. [84] likewise obtained simple form for the fidelities associated with the complete splitting protocol involving teleportation followed by the decodification as

$$F_{GHZS} = \frac{1}{3} \left[2 - p (1 - p) + (1 - p)^{N/2} \right]$$
 (28)

$$F_{WS} = 1 - \frac{p}{3}. (29)$$

The full details of the derivation of the fidelities in Eqs. (26), (27) (28) are provided in Ref.[84].

The evolution dynamics of the teleportation fidelities for the systems under study here, can be obtained as shown in Fig. 6 and 8a by substituting the form of u (Eq.(17)) into Eqs.(26) and (27), and using typical parameter estimates of the FMO complex of P. aestuarii [86]. Likewise the fidelities associated with the complete splitting protocol (teleportation followed by the decodification) obtained using Eqs.(17), (28) and (29) are plotted in Fig. 7 and 8b. Both the GHZ and W_A resource states reach the classical fidelity of 2/3 in the Markovian and non-Markovian regimes, for the two types of fidelities at $t \to \infty$ [84]. The teleportation fidelities associated with the W_A resource states lie above the classical threshold fidelity of 2/3, while those of the GHZ resource states lie below the classical threshold fidelity. The results obtained here are in line with earlier observations by Chaves et. al. [84] that the W_A states display greater robustness than the GHZ states.

The increased revivals in the fidelities with time, for increasing degree of non-Markovian strength, can also be noted for both GHZ and W_A states, with the amplitude of oscillations bounded either from above or below by the classical threshold value. These revivals, appear to last up to time periods of typically 0.5 - 0.7 ps, depending on γ_0 , which is associated with the exciton relaxation time. The oscillations in the fidelity measure is indicative of strong interactions between the excitonic qubit and the phonon reservoir system. Fig. 6a,b,c shows the overall decrease of the teleportation fidelities with the number of qubits N in the GHZ state, however there is also an associated increased oscillations when N is increased at the non-Markovian regime. Unlike the teleportation fidelities, Fig. 7a,b,c shows that the splitting fidelity, F_{GHZS} is more robust to changes in the number of qubits N in the GHZ state. Comparison of the results in Figs. 6, 7 and 8 show that in general, higher fidelities are obtained in the case of the complete splitting protocol involving teleportation followed by the decodification. In particular, there is notable increased oscillations of the fidelities associated with the complete splitting protocol in the non-Markovian regime when γ_0 is increased to 1500 cm^{-1} (see Fig. 8).

Any connection between coherence and fidelity appears to be subtle, and a rigorous link between the two measures have been not demonstrated so far, and is beyond the scope of this work. As the fidelity characterizes the quality of information transmission through the appropriate quantum channels (e.g. excitonic qubit channels of the FMO complex), it would not be naive to link higher fidelities with more robust coherence phenomenon. Using this reasoning, we can attribute coherent oscillations at physiological temperatures to quantum information processing tasks involving teleportation followed by the decodification process involving W_A states of the FMO complex. Such tasks in particular, may become more important at large γ_0 , which is more likely to occur at higher temperatures.

It well known that one antenna complex serves many FMO complexes, and multiple FMOs are connected to a given reaction center, a structural arrangement which allow photosynthetic organisms to most effectively organize cellular resources [2, 4, 94]. Even though the inter-monomer coupling strengths are about one order of magnitude smaller than intra-monomer couplings [14], the three weakly coupled subunits in the FMO photosynthetic complex trimer, can form a larger cluster of excitonic qubits. There also exists the occurrence of massive entangled excitonic qubits of N > 64 across an entire photosynthetic membrane constituting thousands of bacteriochorophylls as determined using atomic force microscopy in Ref. [94].

In summary, there are increased revivals in fidelities in the non-Markovian regime for resource states (GHZ states, W-like states) in contact with a decoherent environment. This can be attributed to the comparatively long phonon reservoir correlation times associated with non-Markovian interactions. Unlike the GHZ states, the W-like states are expected to provide greater resilience to environmental related decoherence during photosynthetic processes. The contribution to global entanglement due to teleportation followed by the decodification tasks in W_A states of the FMO complex appear to play a domineering role during quantum oscillations at physiological temperatures. The possibility of the latter processes accounting for experimental results [18, 20] which show that coherent oscillations persist up to 1 ps at physiological temperatures cannot be ruled out. These results have important implications for multipartite states present in the FMO complex of light-harvesting systems.

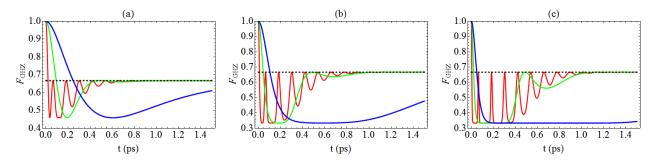


FIG. 6: (a) Teleportation fidelity, F_{GHZ} , as a function of time t (ps) and γ_0 [10 cm⁻¹ (blue line), 50 cm⁻¹ (green line), 1000 cm⁻¹ (red line)] based on the GHZ resource states, using Eq. (26). The detuning parameter is set at δ =0 and N=4. $\Delta\omega$ =80 cm⁻¹ [86] in Eq.(10). The classical fidelity of 2/3 is denoted by dotted lines. (b) Same as in (a) except N=16 (c) Same as in (a) except N=64

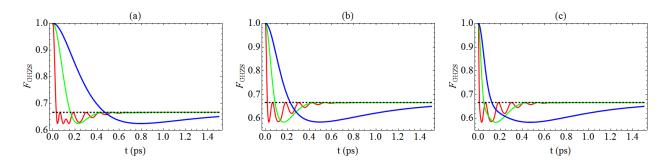


FIG. 7: (a) Quantum information splitting fidelity, F_{GHZS} , as a function of time t (ps) and γ_0 [10 cm⁻¹ (blue line), 50 cm⁻¹ (green line), 1000 cm⁻¹ (red line)] based on the GHZ resource states, using Eq. (28). The detuning parameter is set at $\delta=0$ and N=4. $\Delta\omega=80$ cm⁻¹ [86] in Eq.(10). The classical fidelity of 2/3 is denoted by dotted lines. (b) Same as in (a), except N=16 (c) Same as in (a) except N=64

VI. CONCLUSION

In this work, we examined the exciton entanglement dynamics of the Fenna-Matthews-Olson (FMO) pigment-protein complex from the green sulfur bacteria of the species, Prosthecochloris (P.) aestuarii using typical values of the reservoir characteristics at cryogenic and physiological temperatures [86]. Using the time-convolutionless (TCL) projection operator technique and a Lorentzian spectral density of phonon reservoir, the evolution of the entanglement measure of the excitonic qubit W states is evaluated, showing increased oscillations in the entanglement in the non-Markovian regime. The calculations are repeated for the evolution dynamics of the Meyer-Wallach measure of the N-exciton multipartite state showing that multipartite entanglement can last up to at least 0.5 to 1.0 ps, between the Bchls of the FMO complex, in a decoherent environment.

We have also considered quantum information processing based on teleportation and a complete protocol involving for the GHZ and W_A resource states, within the context of photosynthetic systems. The teleportation fidelities

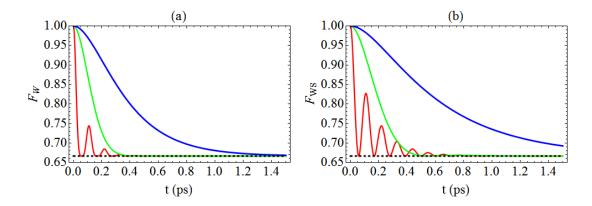


FIG. 8: (a) Teleportation fidelity, F_W , as a function of time t (ps) and γ_0 [10 cm⁻¹ (blue line), 50 cm⁻¹ (green line), 1500 cm⁻¹ (red line)] based on the W_A resource states, using Eq. (27). The detuning parameter is set at $\delta = 0$ and $\Delta \omega = 80$ cm⁻¹ [86] in Eq.(10). The classical fidelity of 2/3 is denoted by dashed lines.

(b) Quantum information splitting fidelity, F_{WS} , as a function of time t (ps) and γ_0 [10 cm⁻¹ (blue line), 50 cm⁻¹ (green line),

(b) Quantum information splitting identy, F_{WS} , as a function of time t (ps) and γ_0 [10 cm | (blue line), 50 cm | (green line), 1500 cm⁻¹ (red line)] based on the W_A resource states, using Eq. (29). The detuning parameter is set at $\delta = 0$ and $\Delta \omega = 80$ cm⁻¹ [86] in Eqs.(10).

associated with the GHZ and W_A resource states associated with the excitonic qubits in the FMO complex of P. aestuarii show increased revivals in the fidelities as the degree of non-Markovian strength is increased. Unlike the GHZ states, the W-like states appear to provide greater resilience to environmental related decoherence during photosynthetic processes. Results indicate that quantum information processing involving teleportation followed by the decodification tasks in W_A states of the FMO complex is likely to account for experimental results which show persistence of coherent oscillations at physiological temperatures.

The results obtained thus far highlight the importance role of several parameters ($\Delta\omega$ associated with the phonon reservoir correlation times, γ_0 associated with the exciton relaxation times, δ associated with the detuning parameter) involved in the long coherence times of multipartite states in the Fenna-Matthews-Olson (FMO) pigment-protein complex of the green sulfur bacteria. In particular the non-Markovian regime appears best suited for occurrence of large coherence times for the model system used in this study. We note however that processes in non-Markovian systems are not well-understood, and further analysis is need to confirm whether non-Markovianity, associated with the backflow of information from the reservoir to the excitonic qubit system, is indeed instrumental in bringing about fast energy transport during photosynthesis.

Lastly, in large light harvesting antennae systems, with intricate network connectivity, coherence between several exciton states involving multipartite states can occur and contribute to the unique ability of these systems to attain robustness against decoherence. The analysis of multipartite states carried out in this work can be extended to estimate the multipartite entanglement measures in photosynthetic systems with alternative forms of spectral functions associated with the environmental couplings. The results obtained in this work may provide useful guidelines for future experimental work involving the detection of multipartite entanglement in photosynthetic systems. In particular, advanced measurement tools involving spectrally resolved, 4-wave mixing measurements [95] may be utilized to examine the remarkable resilience of quantum correlations, and the role of multipartite states in photosynthetic systems in contact with a decoherent environment.

VII. ACKNOWLEDGMENTS

This research was undertaken on the NCI National Facility in Canberra, Australia, which is supported by the Australian Commonwealth Government.

^[1] R. S. Knox, in *Primary Processes of Photosynthesis*, edited by J. Barber, pp. 5597 (Elsevier, Amsterdam, 1977).

^[2] H. Zuber and R. Cogdell, in *Anoxygenic Photosynthetic Bacteria*, edited by R. Blankenship, M. Madigan, and C. Bauer, pp. 315348 (Kluwer Academic, Dordrecht, 1995).

^[3] B. Chance and M. Nishimura, Proc. Nat. Acad. Sci. U.S.A., 46, 19 (1960).

- [4] Light-Harvesting Antennas in Photosynthesis, edited by B. R. Green and W. W. Parson (Springer, New York, 2003).
- [5] V. May and O. Kühn, Charge and Energy Transfer Dynamics in Molecular Systems, 2nd ed. (Wiley-VCH, Berlin, 2004).
- [6] H. van Amerongen, L. Valkunas, and R. van Grondelle, *Photosynthetic Excitons* (World Scientific, Singapore (2000).
- [7] V. Sundström, T. Pullerits and R. van Grondelle, J. Phys. Chem. B 103, 2327 (1999).
- [8] G. R. Fleming and G. D. Scholes GD Nature **431**, 256 (2004).
- R. J. Cogdell, A. Gall A and J. Köhler, Q. Rev Biophys 39, 227 (2006).
- [10] T. Brixner, J. Stenger, H. M. Vaswani, M. Cho, R. E. Blankenship, and G. R. Fleming, Nature, 434, 625 (2005).
- [11] R. E. Fenna and B. W. Matthews, Nature, **258**, 573 (1975).
- [12] A. Camara-Artigas, R. E. Blankenship, J. P. Allen Photosynth. Res. 75, 49 (2003).
- [13] G. S. Engel, T. R. Calhoun, E. L. Read, T.K. Ahn, T. Mancal, Y. C. Cheng, R. E. Blankenship, and G. R. Fleming, Nature, 446, 782 (2007).
- [14] J. Adolphs and T. Renger, Biophys. J. **91**, 2778 (2006).
- [15] M. Wendling, M. A. Przyjalgowski, D. Gülen, S. I. E. Vulto, T. J. Aartsma, R. van Grondelle, and H. van Amerongen, Photosynth. Res. 71, 99 (2002).
- [16] Y. C. Cheng and G. R. Fleming, Annu. Rev. Phys. Chem., **60**, 241 (2009).
- [17] M. Cho, H. M. Vaswani, T. Brixner, J. Stenger, and G. R. Fleming, J. Phys. Chem. B 109, 10542 (2005).
- [18] G. Panitchayangkoon, D. Hayes, K. A. Fransted, J. R. Caram, E. Harel, J. Wen, R. Blankenship, G. S. Engel, Proc. Nat. Acad. Sci. 107, 12766 (2010).
- [19] H. Lee, Y.-C. Cheng, and G. R. Fleming, Science **316**, 1462 (2007).
- [20] E. Collini, C. Y. Wong, K. E. Wilk, P. M. G. Curmi, P. Brumer, and G. D. Scholes, Nature, 463, 644 (2010).
- [21] T. Brixner, J. Stenger, H. M. Vaswani, M. Cho, R. E. Blankenship, and G. R. Fleming, Nature 434, 625 (2005).
- [22] S. Savikhin, D. Buck, W. Struve, Chemical physics, 223, 303, (1997).
- [23] R. J. Sension, Nature **446**, 740 (2007).
- [24] N. Renaud, M. A. Ratner and V. Mujica, J. Chem. Phys. 135, 075102 (2011).
- [25] S. M. Vlaming and R. J. Silbey, J. Chem. Phys. 136, 055102 (2012).
- [26] J. J. Hopfield, Proc. Nat. Acad. Sci. U.S.A., 71, 3640 (1974).
- [27] Th. Förster, Ann. Phys. **437**, 55 (1948).
- [28] M. Mohseni, P. Rebentrost, S. Lloyd and A. Aspuru-Guzik, J. Chem. Phys. 129, 174106 (2008).
- [29] A. Olaya-Castro, Chiu Fan Lee, F. F. Olsen, and N. F. Johnson, Phys. Rev. B 78, 085115 (2008).
- [30] E. N. Zimanyi and R. J. Silbey, J. Chem. Phys. 133, 144107 (2010).
- [31] P. K. Ghosh, A. Y. Smirnov and F. Nori, J. Chem. Phys. **134**, 244103 (2011).
- [32] M. Sarovar, A. Ishizaki, G. R. Fleming and K. B. Whaley, K. B., Nature Physics 6, 462 (2010).
- [33] A. Ishizaki and G. R. Fleming, J. Chem. Phys. 130, 234111 (2009).
- [34] D. Abramavicius and S. Mukamel, J. Chem. Phys. 133, 064510 (2010).
- [35] O. Mülken and T. Schmid, Phys. Rev. E 82, 042104 (2010).
- [36] M. B. Plenio and S. F. Huelga, New J. Phys. **10**, 113019 (2008).
- [37] A. Ishizaki and G. R. Fleming, Proc. Natl. Acad. Sci. USA 106, 107255 (2009).
- [38] P. Rebentrost, M. Mohseni, I. Kassal, S. Lloyd, and A. Aspuru-Guzik, New J. Phys. 11, 033003 (2009).
- [39] F. Caruso, A. W. Chin, A. Datta, S. F. Huelga, and M. B. Plenio, J. Chem. Phys. 131, 105106 (2009).
- [40] F. Caruso, A. W. Chin, A. Datta, S. F. Huelga, and M. B. Plenio, Phys. Rev. A 81, 062346 (2010).
- [41] J. Strümpfer and K. Schulten, J. Chem. Phys. 134, 095102 (2011).
- [42] X. Chen and R. J. Silbey, J. Phys. Chem. B, 132, 205101 (2010).
- [43] M. A. Nielsen and I. L. Chuang, Quantum computation and information (Cambridge University Press, Cambridge, UK, 2000).
- [44] R. Horodecki, P. Horodecki, M. Horodecki, and K. Horodecki, Rev. Mod. Phys. 81, 865 (2009).
- [45] M. Horodecki, P. Horodecki and R. Horodecki, Phys. Lett. A 223, 1 (1996).
- [46] C. Bennett, G. Brassard, C. Crepeau, R. Jozsa, A. Peres, and W. Wootters, Phys. Rev. Lett. 70, 1895 (1993).
- [47] M. Horodecki, P. Horodecki, and R. Horodecki, Phys. Rev. A 60, 1888 (1999).
- [48] S. Popescu, Phys. Rev. Lett. **72**, 797 (1994).
- [49] C.H. Bennett and S.J. Wiesner, Phys. Rev. Lett. 69, 2881 (1992) .
- [50] M. Hillery, V. Bužek, and A. Berthiaume, Phys. Rev. A 59, 1829 (1999).
- [51] C.A. Fuchs, N. Gisin, R.B. Griffiths, C-S. Niu, and A. Peres, Phys. Rev. A 56 1163 (1997) .
- [52] C. H. Bennett, G. Brassard, C. Crepeau, R. Jozsa, A. Peres, W. K. Wootters, Phys. Rev. Lett. 70 1895 (1993).
- [53] V. Coffman, J. Kundu and W. K. Wootters, Phys. Rev. A 61, 052306 (2000).
- [54] H. Ollivier and W. H. Zurek, Phys. Rev. Lett. 88, 017901 (2001).
- [55] L. Henderson and V. Vedral, J. Phys. A 34, 6899 (2001).
- [56] V. Vedral, Phys. Rev. Lett. **90**, 050401 (2003).
- [57] A.P. Majtey, A.R. Plastino and A. Plastino, "New features of quantum discord uncovered by q-entropies" arXiv:1112.4957.
- [58] A. S. Davydov, Theory of Molecular Excitons (Plenum, New York, 1971).
- [59] D. P. Craig and S. H. Walmsley, Excitons in Molecular Crystals (Benjamin Inc., New York, 1968).
- [60] Y. Toyozawa, Optical Processes in Solids (Cambridge, New York, 2003).
- [61] A. Suna, Phys. Rev. **135**, A111 (1964).
- [62] A. Thilagam and J. Singh, Phys. Rev. B 48, 4636 (1993).
- [63] A. Thilagam, Phys. Rev. A 81, 032309 (2010).

- [64] T. Yu and J. H. Eberly, Phys. Rev. Lett. 93, 140404 (2004).
- [65] O. Gühne, F. Bodoky, and M. Blaauboer Phys. Rev. A 78, 060301(R) (2008).
- [66] A. Borras, A. P. Majtey, A. R. Plastino, M. Casas, and A. Plastino, Phys. Rev. A 79, 022108 (2009).
- [67] W. Dür and H. J. Briegel, Phys. Rev. Lett. 92, 180403 (2004).
- [68] L. Aolita, R. Chaves, D. Cavalcanti, A. Acín, and L. Davidovich, Phys. Rev. Lett. 100, 080501 (2008).
- [69] Zhong-Xiao Man, Yun-Jie Xia, and Nguyen Ba An, Phys. Rev. A 78, 064301 (2008).
- [70] O Gühne, F. Bodoky and M. Blaauboer, Phys. Rev. A 78 R060301 (2008).
- [71] A. Borras, A. P. Majtey, A. R. Plastino, M. Casas and A. Plastino, Phys. Rev. A 79 022108 (2009).
- [72] M. Hotta, Phys. Rev. A 80, 042323 (2009).
- [73] E. D Hondt and P. Panangaden, Quantum Inf. Comput. 6, 173 (2006).
- [74] M. Hillery, V. Bužek, and A. Berthiaume, Phys.Rev. A 59, 1829 (1999).
- [75] D. M. Greenberger, M. A. Horne, A. Shimony, and A. Zeilinger, Am. J. Phys. 58, 1131 (1990).
- [76] A. R. R. Carvalho, F. Mintert, and A. Buchleitner, Phys. Rev. Lett. 93, 230501 (2004).
- [77] C. Simon and J. Kempe, Phys. Rev. A 65, 052327 (2002).
- [78] R. H. Dicke, Phys. Rev. **93**, 99 (1954).
- [79] W. Dür, G. Vidal, and J. I. Cirac, Phys. Rev. A 62, 062314 (2000).
- [80] A. Kitaev and J. Preskill, Phys. Rev. Lett. 96 110404 (2006).
- [81] J. Batle, M. Casas, A. R. Plastino and A. Plastino, Phys. Lett. A, 296 251 (2002).
- [82] G. Vidal, R.F. Werner, Phys. Rev. A 65, 032314 (2002).
- [83] D. A. Meyer and N. R. Wallach, J. Math. Phys. 43 4273 (2002).
- [84] R. Chaves and L. Davidovich, Phys. Rev. A 82, 052308 (2010).
- [85] A. P. Majtey, A. Borras, A. R. Plastino, M. Casas and A. Plastino, Int. J. of Quantum Information 8, 505 (2010).
- [86] S. I. E. Vulto, M. A. de Baat, S. Neerken, F. R. Nowak, H. van Amerongen, J. Amesz, and T. J. Aartsma, J. Phys. Chem. B 103, 8153 (1999).
- [87] R. J. W. Louwe, J. Vrieze, A. J. Hoff, T. J. Aartsma, J. Phys. Chem. 101, 11280 (1997).
- [88] S. I. E Vulto, M. A. de Baat, R. J. W. Louwe, H. P. Permentier, T. Neef, M. Miller, H. van Amerongen, T. J. Aartsma, J. Phys. Chem. 102, 9577 (1998).
- [89] A. Thilagam, J. Chem. Phys. 136, 065104 (2012).
- [90] A. Thilagam, J. Phys. A: Math. Theor. 43, 155301 (2010).
- [91] H. P. Breuer and F. Petruccione, The theory of Open Quantum systems (Oxford, Oxford University Press, 2002).
- [92] Z. He, J. Zou, B. Shao and S. Y. Kong, J. Phys. B: At. Mol. Opt. Phys. 43, 115503 (2010).
- [93] A. Thilagam, J. Phys. A: Math. Theor. 42, 335301 (2009).
- [94] M. K. Sener, J D Olsen, C N Hunter, K. Schulten, Proc. Natl. Acad. Sci. USA 104, 15723 (2007).
- [95] D. Segale and V. A. Apkarian, J. Chem. Phys. 135, 024203 (2011).